1   **Revision 1**

2   **Gismondine-Sr, $Sr_4(Al_8Si_8O_{32})\cdot9H_2O$, a new strontium dominant, orthorhombic zeolite**

3   **of the gismondine series from the Hatrurim Complex, Israel.**

4

5   Word Count: 9291

6   Katarzyna Nowak[1*], Georgia Cametti[2], Irina O. Galuskina[1], Yevgeny Vapnik[3]

7   and Evgeny V. Galuskin[1]

8   [1]Institute of Earth Sciences, Faculty of Natural Sciences, University of Silesia, Będzińska 60,

9   41-200 Sosnowiec, Poland;

10   [2]Institute of Geological Sciences, University of Bern, Baltzerstrasse 1+3, 3012 Bern,

11   Switzerland

12   [3]Department of Geological and Environmental Sciences, Ben-Gurion University of the Negev,

13   POB 653, Beer-Sheva 84105, Israel

14   *e-mail: katarzyna.k.nowak@us.edu.pl

15   **Abstract**

16   A new mineral, gismondine-Sr with ordered gismondine framework type ($B22_12$ no. 20,

17   Z= 1; a = 14.0256(2) Å, b = 10.45900(10) Å, c = 13.79360(10) Å), V= 2023.44(4)Å^3) and the

18   following ideal chemical formula $Sr_4(Si_8Al_8O_{32})\cdot9H_2O$ was discovered in amygdaloidal voids

19   of partly melted gehlenite hornfels at Halamish locality, Hatrurim Basin of the Hatrurim

20   Complex, Negev Desert, Israel. Gehlenite hornfels is mainly composed of gehlenite,

21   wollastonite, and garnet of the grossular-andradite-schorlomite series. In a low-temperature

22   association occur minerals such as thomsonite-Ca, flörkeite, analcime and minerals of the

23   tobermorite supergroup. Gismondine-Sr forms spherulitic aggregates up to 180 μm and, rarely,

24   pseudotetragonal bipyramidal crystals up to 50 μm. Empirical crystal chemical formula of

25   gismondine-Sr is as follows $(Sr_{2.02}Ca_{1.09}Ba_{0.02}K_{0.72}Na_{0.62})_{\Sigma4.47}Al_{7.91}Si_{8.09}O_{31.85}\cdot9H_2O$. It is the

26 strontium analog of gismondine-Ca and the second orthorhombic zeolite with the **GIS** structure

27 topology. Crystals are transparent to translucent and feature vitreous lustre. The mineral

28 exhibits a white color, imperfect cleavage in [101] direction, a brittle tenacity, and uneven

29 fracture. The Mohs hardness was estimated at approximately 4. Gismondine-Sr is biaxial

30 negative, $\alpha = 1.488(3)$, $\beta = 1.492(3)$, $\gamma = 1.495(3)$, $2V_{obs} = 70\text{-}80°$. The Raman spectrum is

31 characterized by a band at 465 cm^{-1}, which is also the main band in gismondine-Ca. The

32 structure refinement using SC-XRD ($R_1 = 0.0353$) reveals the ordered distribution of framework

33 cations and the disordered arrangement of extraframework cations. The aluminosilicate

34 framework is built by crankshaft chains with 8-member apertures channels parallel to [101] and

35 [10-1]. In gismondine-Sr, the 8-member rings are elliptically deformed and the T-O-T angle of

36 the upward and downward tetrahedra in the double crankshaft chains is smaller compared to

37 gismondine-Ca. Consequently, a slight rotation of the double crankshaft chains has been

38 noticed. Similar observations have been made in partially dehydrated and the pressure-modified

39 gismondine-Ca. The present study suggests that, in addition to high-pressure and dehydration,

40 the elliptical deformation of the channels in **GIS** also arises as a consequence of the

41 extraframework cations and H_2O content. Thus, the extraframework content influences the

42 aluminosilicate framework leading to the orthorhombic symmetry.

43 Key words: zeolite, **GIS** topology, gismondine, Raman, crystal structure, Hatrurim

44

45 **Introduction**

46 Gismondine-Sr   (IMA2021-043), $Sr_4(Si_8Al_8O_{32})\cdot9H_2O$ ($B22_12$, a =   14.0256(2),

47 $b = 10.45900(10)$, $c = 13.79360(10)$Å, V = 2023.44(4)Å^3) is a new strontium dominant,

48 orthorhombic   analog   of   gismondine.   In   turn,   gismondine   has   been   renamed   to

49 gismondine-Ca and gismondine has become the series name (Miyawaki et al. 2021).

50 Gismondine-Sr was found in amygdaloidal voids in gehlenite pyrometamorphic rocks of the

51   Hatrurim Complex at Halamish Wadi, Hatrurim Basin, Negev Desert, Israel. Gismondine-Sr

52   and other minerals with **GIS** framework type (Table 1) show a structure built by double

53   connected 4-member ring crankshaft chains (Gottardi 1979; Gottardi and Galli 1985;

54   Armbruster and Gunter 2001), which are also present in phillipsite (**PHI**) and merlinoite (**MER**)

55   framework types (Fig. 1). The following seven mineral species are included in gismondine

56   subgroup (Table 1): gismondine-Ca, gismondine-Sr, amicite, garronite-Ca, garronite-Na and

57   gobbinsite. "Gismondine-Ba" described from artificial material is not approved by the

58   Commission on New Minerals, Nomenclature, and Classification - International Mineralogical

59   Association (CNMNC-IMA) (Braithwaite et al. 2001). The highest symmetry of the **GIS**

60   framework topology corresponding to the tetragonal $I4_1/amd$ space group was found in the

61   high-silica synthetic zeolite $Na_{3.6}(Al_{3.6}Si_{12.4})O_{32} \cdot 14H_2O$, a = 9.9989(4), c = 10.0697(4) Å,

62   V=1006.75 Å^3 (Baerlocher and Meier 1972; Håkansson et al. 1990). The topological symmetry

63   of the framework is reduced to orthorhombic due to the cations ordering at the tetrahedral site.

64   Further lowering of the symmetry may occur due to the extraframework cation arrangement

65   (Gottardi and Galli 1985; Armbruster and Gunter 2001). The synthetic monoclinic strontium

66   gismondine was obtained by ion exchange from Na-zeolite (Allen et al. 2002).

67   The new mineral, gismondine-Sr (IMA 2021-043), as well as its name, has been

68   approved by the CNMNC-IMA. The new mineral and the name gismondine-Sr are consistent

69   with the criteria of the new mineral species definition in the zeolite group, clearly specified in

70   "*Recommended nomenclature for zeolite minerals: report of the subcommittee on zeolites of*

71   *the international mineralogical association, commission on new minerals and mineral names*"

72   (Coombs et al. 1997). The holotype material is deposited at the mineralogical collection of the

73   Fersman Mineralogical Museum in Moscow, Russia with the catalog number 97678 for the thin

74   section and 97679 for the rock sample.

75   The aim of this paper is a detailed description of a recently discovered gismondine-Sr,

76   its structure, and the genetic aspects of zeolite mineralization in pyrometamorphic rocks of the

77   Hatrurim Complex.

78

79   **Experimental methods**

80   The semi-quantitative chemical composition of gismondine-Sr, as well as its

81   morphology, was studied using a scanning electron microscope Phenom XL, equipped with an

82   energy dispersive X-Ray spectrometer (Faculty of Natural Science, University of Silesia,

83   Poland). The quantitative chemical analyses were carried out on the microprobe analyzer

84   CAMECA SX100 (Institute of Geochemistry, Mineralogy and Petrology, University of

85   Warsaw, Poland) at 15 kV and 10 nA, spot size was defocused and was 5 μm. A larger spot

86   size has not been used because of the relatively small grain size. The following lines and

87   standards were used: Na$K\alpha$ = albite; Si$K\alpha$ = diopside; Al$K\alpha$ = orthoclase; K$K\alpha$ = orthoclase;

88   Ca$K\alpha$ = diopside; Fe$K\alpha$ = Fe$_2$O$_3$; Sr$L\alpha$ = celestine, Ba$L\alpha$ = baryte.

89   The Raman spectrum was obtained on a confocal Raman Microscope WITec alpha

90   300R (Faculty of Natural Science, University of Silesia, Poland), equipped with an air-cooled

91   488 nm laser and a CCD camera working at -61℃. The Raman signal was recorded with an

92   optical fiber 30 μm in diameter and a monochromator with a 600 mm^{-1} grating. The laser power

93   was ≈ 10 mW on the sample surface. The time of measurement was 3 s with an accumulation

94   of 25 scans and a spectral resolution of 3 cm^{-1}. The monochromator was calibrated using the

95   Raman scattering line of a silicon plate (520.7 cm^{-1}). Spectral software package GRAMS

96   (Galactic Industries Corporation, New Hampshire, USA) was used for data processing. The

97   fitting of Raman bands was performed using a Gauss-Lorentz cross-product function with

98   preservation of the rule of minimum number of component bands.

4

99   Diffraction data were collected using a Rigaku Synergy-S diffractometer equipped with

100   a dual micro-focused source and a Hypix detector. CuKα radiation (λ = 1.540598 Å) was chosen

101   because of the small size of the crystals (0.07×0.04×0.03 mm). Preliminary lattice parameters

102   and the orientation matrix were obtained from three sets of frames. Final diffraction data were

103   collected with ω scans at different φ settings. The software package CrysalisPro 40.29a was

104   used for the data reduction and absorption correction. The structure was solved by direct

105   methods using SHELXS (Sheldrick 2008). The structural refinement was carried out by using

106   SHELXL (Sheldrick 2015) and neutral atomic scattering factors for all atoms. The structure

107   was refined as an inversion twin, with fractional volume contribution expressed by the BASF

108   parameter (Sheldrick 2015) equal to 0.16(4).

109   Because gismondine-Sr occurs only in small concentration and it forms intimate

110   intergrowth with other zeolites it was not possible to collect experimental X-ray powder

111   diffraction data (PXRD). The PXRD pattern have been calculated more reliably from the results

112   of the single-crystal structure refinement using PowderCell 2.4 program (Kraus and Nolze

113   1996). The calculated pattern of gismondine-Sr and gismondine-Ca (Wadoski-Romeijn and

114   Armbruster 2013) are given in Supplemental Tables S1 and S2, respectively. The distinction

115   between orthorhombic and monoclinic symmetry of gismondine is possible using the powder

116   diffraction patterns.

117

Geological settings and paragenesis

119   The Hatrurim Complex, known as Mottled Zone, is composed of high-temperature

120   metamorphic rocks and products of their low-temperature alteration spread on both sides of the

121   Dead Sea Transform Fault in Israel, Palestine Autonomy, and Jordan (Fig. 2a; Bentor 1960;

122   Gross 1977; Burg et al. 1992, 2000). High-temperature rocks are represented by spurrite marble,

123   larnite pseudoconglomerates and gehlenite hornfelses formed at the sanidinite facies conditions

5

124   after sedimentary protolith. Until now, despite many mineralogical studies over the last ten

125   years, there is no scientific consensus on the genesis of these rocks. The most disputable issue

126   is the source of heat energy. One of the theories establishes that the heat energy accrues from

127   the combustion of bituminous chalk organic matter (Gross 1977; Geller et al. 2012; Galuskina

128   et al. 2014). The latest conception associates the origin of pyrometamorphic processes with

129   neotectonic mud volcanism and methane burning (Sokol et al. 2008, 2010; Novikov et al. 2013;

130   Galuskina et al. 2014). Last year's investigations showed that during formation of high-

131   temperature rocks, the earlier formed minerals („clinker association") react with combustion

132   by-products, leading to a significantly greater variety of mineral species (Galuskina et al. 2014,

133   2017; Galuskin et al. 2015, 2016).

134   The pyrometamorphic rocks contain cracks, voids, and veins filled by low-temperature

135   mineralization formed due to hydrothermal alteration and weathering (Kolodny et al. 2014;

136   Juroszek et al. 2020, Kruszewski et al. 2021). Gismondine-Sr was found in small amygdaloidal

137   voids of partially melted gehlenite hornfels at wadi Halamish locality (N31°09′42″

138   E35°17′29″), which is located at the southern part of the Hatrurim Basin - the largest exposed

139   field of pyrometamorphic rocks of the Hatrurim Complex in Israel (Burg et al. 1992, 2000;

140   Vapnik et al. 2007; Geller et al. 2012). The investigated material was collected in a marginal

141   part of grey basalt-like gehlenite-wollastonie paralava, which contains sulphide globules

142   (Galuskina et al. in preparation). These pyrometamorphic rocks occur as irregular lenses low-

143   T calcium-hydrosilicate rocks and stratigraphically they correspond to the lower part of the

144   Ghareb Formation. Hornfels is composed of gehlenite, wollastonite, rankinite, and garnet of the

145   grossular-andradite-schorlomite series (Fig. 3). Accessory minerals are represented by

146   fluorapatite, perovskite, minerals of magnesioferrite-trevorite-magnetite-maghemite series, and

147   hematite (Fig. 3). Additionally, in amygdaloidal voids occur other zeolites such as gismondine-

148   Ca, thomsonite-Ca, and two generations of flörkeite forming before and after gismondine-Sr

6

149   (Fig. 3c). Analcime and minerals of the tobermorite supergroup, which surrounded the voids,

150   are also present in association (Fig. 3b).

151   Furthermore, gismondine-Sr was found in voids of gehlenite hornfels from Zohar Wadi

152   near the road Arad - Dead See (Fig. 2b). The association of main minerals is similar for both

153   localities.

154

155   **Physical and optical properties of gismondine-Sr**

156   Gismondine-Sr forms spherulitic aggregates up to 180 μm in the largest dimension

157   filling amygdaloidal voids and (Fig. 3c). Pseudotetragonal bipyramidal crystals up to 50 μm are

158   rarely observed. Its color and streak are white. Crystals are transparent to translucent and feature

159   vitreous lustre. It does not exhibit fluorescence. Imperfect cleavage is observed in the [101]

160   direction. The tenacity is brittle, and the fracture is uneven. The Mohs hardness was estimated

161   at approximately 4, and the mean micro-hardness is 302(8) kg/mm^2. The range is 289-325

162   kg/mm^2 with VHN loaded 25 g. Gismondine-Sr is gradually dissolved in 10% HCl.

163   Measurements of density could not be performed because of a large number of microcracks and

164   a high degree of hydration. Density, $D_{calc.}$ = 2.301 g·cm^{-3}, was calculated on the basis of the

165   empirical formula of the holotype and the unit cell volume refined from the SC-XRD data.

166   Pleochroism is not observed. Gismondine-Sr is negative biaxial, α = 1.488(3), β = 1.492(3), γ

167   = 1.495(3), $2V_{obs}$ = 70-80°, $2V_{calc}$ = 81.8°. Dispersion is weak. The optical orientation is

168   consistent with the cell vectors. The Gladstone-Dale compatibility index based on the empirical

169   values of the oxides, and the calculated H_2O content is 1 – (K_P/K_C) = -0.004 (superior)

170   (Mandarino 1981).

171

172   **Chemical composition**

7

173   The results of EMPA chemical analysis are presented in Table 2. The empirical formula

174   is calculated on the basis of 16 *T-sites* within the framework. The water content was calculated

175   based on stoichiometry, which is consistent with the SC-XRD data. The empirical formula of

176   gismondine-Sr from the type locality (symbol C1 in Table 2) could be written as:

177     $(Sr_{2.02}Ca_{1.09}Ba_{0.02}K_{0.72}Na_{0.62})_{\Sigma 4.47}Al_{7.91}Si_{8.09}O_{31.85} \cdot 9H_2O$. The empirical formula of gismondine-

178   Sr   from   Zohar   (C2   in   Table   2)   is   as   follows:

179     $(Sr_{1.79}Ca_{1.15}Ba_{0.03}K_{0.81}Na_{0.50})_{\Sigma 4.28}Al_{7.93}Si_{8.05}O_{31.62} \cdot 9H_2O$.   The   end-member   formula   of

180   gismondine-Sr is $Sr_4Al_8Si_8O_{32} \cdot 9H_2O$ (see Discussion).

181

182   **Raman spectroscopy**

183   The Raman spectra of gismondine-Sr are presented in Fig. 4. The main bands and their

184   assignments are given in Table 3. The range 323-500 cm^{-1} corresponds to symmetric bending

185   vibrations of T-O-T in rings (Dutta and Del Barco 1988; Dutta et al. 1991; Knops-Gerrits et al.

186   1997; Yu et al. 2001; Mozgawa et al. 2005). Variations in bands intensity, depending on the

187   crystal orientation, is visible in this range (Fig. 4a,b), for example, the band at 396 cm^{-1}. Bands

188   between 671 cm^{-1} and 721 cm^{-1} could be attributed to symmetric stretching modes T-O-T (Yu

189   et al. 2001; Mozgawa et al. 2005). Bands related to symmetric and antisymmetric stretching

190   vibrations of T-O in tetrahedra are in the range 969-1083 cm^{-1} (Dutta and Del Barco 1988; Dutta

191   et al. 1991; Knops-Gerrits et al. 1997; Yu et al. 2001; Gujar et al. 2005). Other bands in the

192   spectrum are assigned to water molecules. The band around 1660 cm^{-1} corresponds to bending

193   vibrations, and bands between 3130 cm^{-1} and 3600 cm^{-1} are attributed to stretching vibrations

194   of water (Tsai et al. 2021). The gismondine-Sr Raman spectrum confirms the gismondine

195   structure topology (Tsai et al. 2021, Fig. 4).

196

197   **Crystallography and structure description**

8

198   The crystal structure of gismondine-Sr ($B22_12$, $a = 14.0256(2)$ Å, $b = 10.45900(10)$ Å, $c =$

199   13.79360(10) Å, $V = 2023.44(4)$Å^3) was refined from the SC-XRD data. Details of the

200   experiment and parameters of structure refinement are given in Table 4. The reflections were

201   indexed in a C-centred orthorhombic lattice. After data reduction, the analysis of the intensities

202   pointed to the space group $C222_1$(#20). The non-standard setting $B22_12$ was chosen for

203   similarity with the unit-cell of a high-temperature modification of gismondine (Vezzalini et al.

204   1993; Wadoski-Romeijn and Armbruster 2013). Firstly, the framework atoms (Si, Al, O) were

205   located. According to chemical analysis (Si/Al = 1) and Löewenstein rule (Löewenstein 1954),

206   Si and Al are orderly distributed at distinct tetrahedral sites (Si1, Si2, Si3 and Al1, Al2, Al3, for

207   Si and Al, respectively; Table 5), which were assigned to the basis of interatomic T-O distances

208   (mean distances T(Al)-O = 1.73Å and T(Si)-O = 1.61Å, Table 6). Framework oxygen atoms

209   occupy eight sites: O1-O8 (Table 5). After the first cycle of refinement, two strong peaks

210   appeared in difference-Fourier maps. These peaks were added to the structural model ($C1$ and

211    $C2$ sites) and refined with Sr scattering factors. Additional residual electron density was found

212   very close (distances in the range of 0.5-1.0 Å) to the $C1$ and $C2$ sites. Such residual electron

213   density was modelled by low-occupied sites ($C1A$, $C1B$, $C1C$ and $C2A$, $C2B$) refined with Ca,

214   Na, and K scattering factors, respectively (Table 5). The assignment of atomic species to each

215   crystallographic site was not straightforward due to the structural disorder and the low

216   population of these sites. The best model, which was consistent with the chemical composition,

217   achieved the quality of the structural refinement $R_1 = 0.0353$.

218   **GIS** structure is composed of 4-membered rings tetrahedra, which form double

219   crankshaft chains (defined as dcc, Fig. 5). The dcc chains are connected to each other and create

220   double four-membered rings, which originate two systems of channels with 8-membered ring

221   apertures. These channels run parallel to [101] and [10-1] (Fig. 5), and they are connected by

222   2_1 axes parallel to [010]. At the intersection of two system channels occur t-gsm cavities, which

9

223 are built by six four-membered rings and four eight-membered rings (notation $4^6 8^4$) (Figs. 6,7,

224 Alberti and Vezzalini 1979).

225   In gismondine-Sr, extraframework cations and H_2O are disorderly distributed at

226 partially occupied sites in the *t-gsm* cavity (Fig. 6, Table 5). Strontium is the dominant

227 extraframework cation, located at sites $C1$ and $C2$ within two adjacent cages, respectively. Each

228 of these cages hosts 0.6 Sr disordered over two symmetry-equivalent sites (Figs. 6b, 7a,b),

229 whose simultaneous occupation is prevented due to the excessively short distances between

230 them (approximately 2.8 Å Table 6). The remaining extraframework cations (Ca, K and Na) do

231 not equally distribute between two adjacent *t-gsm* cavities (Fig. 6b). One cavity is occupied by

232 Ca, Na, and K at $C1A$, $C1B$, and $C1C$, respectively (Fig. 7a), whereas the adjacent one - by Ca

233 and K at $C2A$ and $C2B$ sites, respectively (Fig. 7b, Table 5). Thus, although the refined

234 occupancy of $C1$ and $C2$ converged to the same value, the arrangement of other cations (K, Ca,

235 and Na) slightly differs, and the two adjacent *t-gsm* cavities are not symmetry-equivalent. H_2O

236 is also disordered at partially occupied eight sites (Table 5), which have no simultaneous full

237 occupancy because of the excessively short distances from each other.

238 **Discussion**

239   Gismondine-Sr is one of the few zeolites which contain strontium as dominant

240 extraframework cation and the first strontium zeolite with the **GIS** framework type (Gottardi

241 1979; Gottardi and Galli 1985; Smith 1988; Armbruster and Gunter 2001; Baerlocher et al.

242 2007). After gobbinsite, gismondine-Sr is the second **GIS** zeolite, with the orthorhombic

243 symmetry (Gatta et al. 2010). The unit cell of gismondine-Sr is related to the monoclinic cell

244 of gismondine-Ca by the matrix transformation 101/010/10-1, which corresponds to rotation by

245 an angle of 45° around the b axis and leads to an increase in the a and c parameters. As a result,

246 gismondine-Sr has almost doubled the unit cell volume with respect to gismondine-Ca (Table

247 7, Vezzalini et al. 1993). Both gismondine-Ca and gismondine-Sr are characterized by an

248 ordered Si/Al distribution of the tetrahedral framework. However, within the channels of

249 gismondine-Sr the extraframework cations and H_2O molecules are disorderly distributed

250 (Tables 5, 6, Figs. 5,6).

251   The comparison of gismondine-Sr and gismondine-Ca frameworks showed that T-O-T

252 angle between the upward and downward tetrahedra in the double crankshaft chains is smaller

253 in gismondine-Sr (Fig. 1b, Fig. 4b; mean T-O-T angle in gis-Sr: 140.47; mean T-O-T angle in

254 gis-Ca: 143.32). However, no significant changes in the value of angles in the 4-member rings

255 building the double crankshaft chains have been observed, suggesting their quasi-rigid

256 behavior. In contrast to gismondine-Ca, in gismondine-Sr the ellipticity ratio in the two 8-

257 membered channels are similar (Table 7). Consequently, a slight rotation of the double

258 crankshaft chains in gismondine-Sr was observed (Fig. 8). The tilting occurs around bridging

259 O atoms between the upward and downward tetrahedra in the double crankshaft chain, which

260 behaves as hinges within the framework (Fig. 1b, Fig. 4b; Gatta and Lee 2014). The framework

261 of gismondine-Sr is similar to partially dehydrated gismondine-Ca (Vezzalini et al. 1993;

262 Wadoski-Romeijn and Armbruster 2013; Fig.8c). Moreover, deformations of partially

263 dehydrated gismondine-Ca are similar to deformations of pressure-induced gismondine-Ca,

264 which was reported by Betti et al. (2007) and Ori et al. (2008). The ellipticity of the 8-membered

265 channels increases with the degree of dehydration or pressure, respectively. Moreover, the

266 decrease of the T-O-T angle of the crankshaft chain was also observed (Vezzalini et al. 1993;

267 Betti et al. 2007; Fig. 8c). The Raman spectrum of gismondine-Sr shows no change in the main

268 band, which vibrates at 465 cm^{-1} (Table 3) as in the case of gismondine-Ca. Thus, in agreement

269 with the quasi-rigid behavior of the 4-member rings, the main band could be attributed to T-O-

270 T vibration of the 4-member rings. Furthermore, its frequency is independent from the T-O-T

271 angle in the double crankshaft chains (Table 7, Fig. 4). The bands from 8-member rings could

272 appear on the spectrum (Fig. 4) at 396 cm^{-1} according to the rule that larger rings correspond to

273   lower frequencies (Dutta and Del Barco 1988; Dutta et al. 1991; Knops-Gerrits et al. 1997; Yu

274   et al. 2001). Its variations of intensity (Fig. 4a,b) could be related to the orientation of the

275   channels with regard to the laser beam.

276   Zeolites of the gismondine group (Table 1) reveal different extraframework cations and

277   different Si/Al ratios. Gismondine-Ca, amicite and gismondine-Sr stand out from this group by

278   the Si/Al ratio equal to one. The isomorphic substitution scheme of gismondine-Ca for

279   gismondine-Sr is as follows: $Ca^{2+} \rightarrow Sr^{2+}$. Additionally, the experimental data indicate

280   monoclinic symmetry for the pure strontium gismondine (Allen et al. 2002), as it is the case

281   with gismondine-Ca and gismondine-Ba (Fischer 1963; Braithwaite et al. 2001). However, the

282   content of the monovalent cations in the composition of the investigated gismondine-Sr is

283   significantly different compared to gismondine-Ca, in which monovalent cations are present in

284   negligible amounts (Vezzalini and Oberti 1984). The presence of roughly equal content of K

285   and   Na   in   the   composition   of   the   holotype   gismondine-Sr,

286    $(Sr_{2.02}Ca_{1.09}Ba_{0.02}K_{0.72}Na_{0.62})_{\Sigma 4.47}Al_{7.91}Si_{8.09}O_{31.85}\cdot 9H_2O$ is indicative of formal existence of a

287   solid solution between gismondine-Sr and amicite $K_4Na_4(Al_8Si_8O_{32})\cdot 10H_2O$. Based on the end-

288   member   formulas   of   gismondine-Ca $Ca_4(Al_8Si_8O_{32})\cdot 16H_2O$,   gismondine-Sr

289    $Sr_4(Al_8Si_8O_{32})\cdot 9H_2O$ and amicite $K_4Na_4(Al_8Si_8O_{32})\cdot 10H_2O$, the scheme of the substitutions

290   could be presented as follows: $H_2O + Ca^{2+}/Sr^{2+} \rightarrow 2(Na^+/K^+)$. Thus, besides monoclinic

291   symmetry, gismondine-Sr without monovalent extraframework cations is characterized by a

292   higher water content compared to the presented data. The general zeolite formula with the

293   gismondine framework type and Si/Al ratio equal to one could be: $(D,M)_{4-8}(Si_8Al_8)\cdot nH_2O$,

294   where M is monovalent and D is divalent cations. The simplified formula of gismondine-Sr

295   derived from the EMPA and structural data can be presented as $(D_{3.1}M_{1.8})_{\Sigma 4.9}(Al_8Si_8O_{32})\cdot 9H_2O$,

296   i.e. the $D_4(Al_8Si_8O_{32})\cdot 9H_2O$ end-member is more than 77%. Strontium is significantly

12

297 predominant over calcium at the D site, so the ideal formula of gismondine-Sr would be

298 $Sr_4(Al_8Si_8O_{32})\cdot 9H_2O$.

299 Based on the filling voids (Fig. 3c), the sequence of zeolite crystallization in the voids

300 of gehlenite-wollastonite paralava could be presented as thomsonite-Ca,

301 $NaCa_2(Al_5Si_5O_{20})\cdot 6H_2O$ (**THO** framework); flörkeite, $K_3Ca_2Na(Al_8Si_8O_{32}\cdot 12H_2O$ (**PHI**

302 framework); gismondine-Sr, $Sr_4(Al_8Si_8O_{32}\cdot 9H_2O$ (**GIS** framework) and again flörkeite.

303 Moreover, analcime, $Na(AlSi_2O_6)\cdot H_2O$ (**ANA** framework) is the last zeolite of the

304 crystallization sequence in pyrometamorphic rocks of the Hatrurim Complex. The presented

305 sequence implies that the formation of gismondine-Sr is conditioned by a one-time appearance

306 of high Sr content in the crystallization environment. The association of flörkeite and

307 gismondine-Sr suggests very low-temperature (<100°C) conditions of crystallization of these

308 zeolites (Lengauer et al. 2009).

309 The controversial question is the origin of the strontium in the environment. As shown

310 by Geller et al. (2012) and Sokol et al. (2014, 2019), the sedimentary rocks, protolith of

311 gehlenite hornfels, contain carbonates enriched with strontium. We suggest that during

312 processes of pyrometamorphism, strontium from carbonates has been released. The relatively

313 elevated strontium content was recorded in bulk analyses of pyrometamorphic rocks, but it is

314 rather dispersed in rock-forming minerals, especially in fluorapatite-fluorellestadite and baryte

315 (Juroszek et al. 2018; Sokol et al. 2019).

316

Implication

318 Zeolites are the most common microporous materials in nature. They are characterized

319 by selective cation-exchange capacity, reversible hydration and dehydration, catalytic activity,

320 and sorption of molecules induced by pressure, the investigation of which has seen rapid

321 development in the past decade (Gatta 2003; Betti et al. 2007; Ori et al. 2008; Arletti et al. 2017;

322 Gatta et al. 2018). Zeolites with **GIS** framework type are used as detergent builders (Adams et

323 al. 1995, 1997) and they received attention because of the high framework flexibility (Betti et

324 al. 2007; Gatta and Lee 2014; Arletti et al. 2017; Chukanov et al. 2020). Nevertheless, despite

325 many studies on zeolites synthesis and ion exchange properties, in literature data on Sr^{2+} in **GIS**

326 are scarce (Taylor 1964; Mimura and Akiba 1993; Dyer et al. 2006; Kwon et al. 2021).

327 Previously conducted high-pressure experiments showed that the deformation

328 mechanisms of the structure are conditioned by the topological configuration of the

329 aluminosilicate framework (Gatta 2003; Gatta and Lee 2014; Gatta et al. 2018). However, the

330 influence of the Si/Al distribution and the extra-framework cations on the deformation has not

331 been investigated in detail. The channels content is also responsible for the compressibility of

332 the cavities and therefore can lead to different deformation mechanisms under non-ambient

333 conditions. The present study suggested that, in addition to high-pressure and dehydration

334 (Vezzalini et al. 1993; Wadoski-Romeijn and Armbruster 2013; Gatta and Lee 2014), the

335 elliptical deformation of the channels in **GIS** also arises as a consequence of the extraframework

336 cations and H_2O content. In conclusion, the extraframework content, i.e. the type of

337 extraframework cations in *t-gsm* cages of gismondine-Sr, influences the aluminosilicate

338 framework leading to the orthorhombic symmetry. In general, the gismondine framework type

339 is extraordinarily flexible and could sorb ions with a wide range of ionic radii at the expense of

340 changing framework symmetry.

341

342 **Acknowledgment**

14

346   no.   UMO-2019/35/O/ST10/01015.   The   Swiss   National   Science   Foundation   (SNF)

347   is acknowledged for for the R'Equip grant n. 206021_177033 awarded to P. Macchi.

348

349   **References cited**

350   Adams, C.J., Araya, A., Carr, S.W., Chapple, A.P., Graham, P., Minihan, A.R., and Osinga,

351   T.J. (1995) Zeolite map: A new detergent builder. In Studies in Surface Science and

352   Catalysis. Elsevier, 98, 206–207.

353   Adams, C.J., Araya, A., Carr, S.W., Chapple, A.P., Franklin, K.R., Graham, P., Minihan,

354   A.R., Osinga, T.J., and Stuart, J.A. (1997) Zeolite map: The new detergent zeolite. In

355   Studies in Surface Science and Catalysis. Elsevier, 105, 1667–1674.

356   Alberti, A., and Vezzalini, G. (1979) The crystal structure of amicite, a zeolite. Acta

357   Crystallographica Section B Structural Crystallography and Crystal Chemistry, 35, 2866–

358   2869.

359   Allen, S., Carr, S., Chapple, A., Dyer, A., and Heywood, B. (2002) Ion exchange in the

360   synthetic gismondine, zeolite MAP. Physical Chemistry Chemical Physics, 4, 2409–

361   2415.

362   Arletti, R., Giacobbe, C., Quartieri, S., and Vezzalini, G. (2017) The Influence of the

363   Framework and Extraframework Content on the High Pressure Behavior of the GIS Type

364   Zeolites: The Case of Amicite. Minerals, 7, 18.

365   Armbruster, T., and Gunter, E. (2001) Crystal Structures of Natural Zeolites. In Natural

366   Zeolites: Occurrence, properties, applications Vol. 45, pp. 1–68. Mineralogical Society of

367   America; Geochemical Society.

368   Baerlocher, C., and Meier, W.M. (1972) The crystal structure of synthetic zeolite Na-P 1, an

369   isotype of gismondine. Zeitschrift für Kristallographie, 135, 339–354.

370   Baerlocher, C., McCusker, L.B., and Olson, D.H. (2007) Atlas of zeolite framework types,

371   6th rev. ed., 398 p. Elsevier, Amsterdam.

372   Bentor, Y.K. (1960) Israel. In Lexique Stratigraphique International, Asie.

373   Betti, C., Fois, E., Mazzucato, E., Medici, C., Quartieri, S., Tabacchi, G., Vezzalini, G., and

374   Dmitriev, V. (2007) Gismondine under HP: Deformation mechanism and re-organization

375   of the extra-framework species. Microporous and Mesoporous Materials, 103, 190–209.

376   Bowen, N.L. (1940) Progressive metamorphism of siliceous limestone and dolomite. Journal

377   of Geology 48, 225-274.

378   Braithwaite, R.S.W., Dyer, A., and Wilson, J.I. (2001) Gismondine-Ba, a zeolite from the

379   weathering of slag. Journal of the Russell Society, 7, 83–85.

380   Britvin, S. N., Murashko M. N., Vapnik Y., Polekhovsky Yu. S., Krivovichev S. V. (2017)

381   Barringerite Fe_2P from Pyrometamorphic Rocks of the Hatrurim Formation, Israel.

382   Geology of ore deposits, 59,7, 619-625.

383   Britvin, S. N., Murashko M. N., Vapnik Y., Polekhovsky Y. S., Krivovichev S. V.,

384   Vershchagin O. S., Shilovskikh V. V., Vlasenko N. S., Krzhizhanovskaya M. G. (2020)

385   Halamishite, Ni_5P_4, a new terrestrial phosphide in the Ni-P system. Physics and

386   Chemistry of minerals, 47.

387   Burg, A., Starinsky, A., Bartov, Y., and Kolodny, Y. (1992) Geology of the Hatrurim

388   Formation ("Mottled Zone") in the Hatrurim basin. Israel Journal of Earth Sciences, 40,

389   107–124.

390   Burg, A., Kolodny, Y., and Lyakhovsky, V. (2000) Hatrurim-2000: The "Mottled Zone"

391   revisited, forty years later. Israel Journal of Earth Sciences, 48, 209–223.

392   Chukanov, N.V., Kazheva, O.N., Chervonnaya, N.A., Varlamov, D.A., Ermolaeva, V.N.,

393   Pekov, I.V., and Shilov, G.V. (2020) Ion-exchange properties of the natural zeolite

394   amicite. Macedonian Journal of Chemistry and Chemical Engineering, 39, 207.

16

395   Coombs, D., Alberti, A., Armbruster, T., Artioli, G., Colella, C., Galli, E., Grice, J.D., Liebau,

396   F., Mandarino, J.A., Minato, H., and others (1997) Recommended nomenclature for

397   zeolite minerals: report of the subcommittee on zeolites of the international mineralogical

398   association, commission on new minerals and mineral names. The Canadian

399   Mineralogist, 35, 1571–1606.

400   Dutta, P.K., and Del Barco, B. (1988) Raman spectroscopy of zeolite A: influence of

401   silicon/aluminum ratio. The Journal of Physical Chemistry, 92, 354–357.

402   Dutta, P.K., Rao, K.M., and Park, J.Y. (1991) Correlation of Raman spectra of zeolites with

403   framework architecture. The Journal of Physical Chemistry, 95, 6654–6656.

404   Fischer, K. (1963) The crystal structure determination of the zeolite gismondite

405       $CaAl_2Si_2O_84H_2O$. Mineralogical Notes, 664–672.

406   Galli, E., Gottardi, G., Pongiluppi, D. (1979) The crystal structure of the zeolite merlinoite.

407   Neues Jahrbuch für Mineralogie, Monatshefte, 1979, 1-9.

408   Galuskin, E.V., Gfeller, F., Armbruster, T., Galuskina, I.O., Vapnik, Y., Murashko, M.,

409   Włodyka, R., and Dzierżanowski, P. (2015) New minerals with a modular structure

410   derived from hatrurite from the pyrometamorphic Hatrurim Complex. Part I.

411   Nabimusaite, $KCa_{12}(SiO_4)_4(SO_4)_2O_2F$, from larnite rocks of Jabel Harmun, Palestinian

412   Autonomy, Israel. Mineralogical Magazine, 79, 1061–1072.

413   Galuskin, E.V., Galuskina, I.O., Gfeller, F., Krüger, B., Kusz, J., Vapnik, Y., Dulski, M., and

414   Dzierżanowski, P. (2016) Silicocarnotite, $Ca_5[(SiO_4)(PO_4)](PO_4)$, a new „old'' mineral

415   from the Negev Desert, Israel, and the ternesite–silicocarnotite solid solution: indicators

416   of high-temperature alteration of pyrometamorphic rocks of the Hatrurim Complex,

417   Southern Levant. European Journal of Mineralogy, 28, 105–123.

418 Galuskina, I.O., Vapnik, Y., Lazic, B., Armbruster, T., Murashko, M., and Galuskin, E.V.

419   (2014) Harmunite $CaFe_2O_4$: A new mineral from the Jabel Harmun, West Bank,

420   Palestinian Autonomy, Israel. American Mineralogist, 99, 965–975.

421 Galuskina, I.O., Galuskin, E.V., Vapnik, Y., Prusik, K., Stasiak, M., Dzierżanowski, P., and

422   Murashko, M. (2017) Gurimite, $Ba_3(VO_4)_2$ and hexacelsian, $BaAl_2Si_2O_8$ – two new

423   minerals from schorlomite-rich paralava of the Hatrurim Complex, Negev Desert, Israel.

424   Mineralogical Magazine, 81, 1009–1019.

425 Galuskina, I.O., Krüger, B., Galuskin, E.V., Krüger, H., Vapnik, Y., Murashko, M., Banasik,

426   K., Agaakhanov, A.A., Pauluhn, A., Olieric, V. Zoharite, $Ba_6Fe^{2+}(Fe^{2+}_{16}Cu^+_8)S_{27}$, and

427   gmalimite, $K_6\square Fe^{2+}_{24}S_{27}$ - new minerals from gehlenite-wollastonite paralava, Hatrurim

428   Complex, Israel. Contribution to the improvement of djerfisherite group end-member

429   systematics, in preparation.

430 Gatta, G. (2003) New insights on high-pressure behaviour of microporous materials from X-

431   ray single-crystal data. Microporous and Mesoporous Materials, 61, 105–115.

432 Gatta, G.D., and Lee, Y. (2014) Zeolites at high pressure: A review. Mineralogical Magazine,

433   78, 267–291.

434 Gatta, G.D., Birch, W.D., and Rotiroti, N. (2010) Reinvestigation of the crystal structure of

435   the zeolite gobbinsite: A single-crystal X-ray diffraction study. American Mineralogist,

436   95, 481–486.

437 Gatta, G.D., Lotti, P., and Tabacchi, G. (2018) The effect of pressure on open-framework

438   silicates: elastic behaviour and crystal–fluid interaction. Physics and Chemistry of

439   Minerals, 45, 115–138.

440 Gatta, G.D., Cappelletti, P., Rotiroti, N., Slebodnick, C., Rinaldi, R. (2009) New insights into

441   the crystal strucutre and crystal chemistry of the zeolite phillipsite. American

442   Mineralogist, 94, 190-199.

443   Geller, Y.I., Burg, A., Halicz, L., and Kolodny, Y. (2012) System closure during the

444   combustion metamorphic "Mottled Zone" event, Israel. Chemical Geology, 334, 25–36.

445   Gottardi, G. (1979) Topologic symmetry and real symmetry in framework silicates.

446   Mineralogy and Petrology, 26, 39–50.

447   Gottardi, G., and Galli, E. (1985) Natural zeolites.

448   Grice, J.D., Rowe, R., and Poirier, G. (2016) Garronite-Na, A New Zeolite Species From

449   Mont Saint-Hilaire, Québec. The Canadian Mineralogist, 54, 1549–1562.

450   Gross, S. (1977) The mineralogy of the Hatrurim Formation, Israel. Geological Survey of

451   Israel Bulletin, 70.

452   Gujar, A.C., Moye, A.A., Coghill, P.A., Teeters, D.C., Roberts, K.P., and Price, G.L. (2005)

453   Raman investigation of the SUZ-4 zeolite. Microporous and Mesoporous Materials, 78,

454   131–137.

455   Håkansson, U., Fälth, L., and Hansen, S. (1990) Structure of a high-silica variety of zeolite

456   Na-P. Acta Crystallographica Section C Crystal Structure Communications, 46, 1363–

457   1364.

458   Hirsch, F., Burg, A., Avani, Y. (2008) Geological Map of Israel 1:50 000 Arade Sheet 15-IV,

459   Geological Survey.

460   Juroszek, R., Krüger, B., Galuskina, I., Krüger, H., Vapnik, Y., and Galuskin, E. (2020)

461   Siwaqaite, $Ca_6Al_2(CrO_4)_3(OH)_{12} \cdot 26H_2O$, a new mineral of the ettringite group from the

462   pyrometamorphic Daba-Siwaqa complex, Jordan. American Mineralogist, 105, 409–421.

463   Juroszek, R., Krüger, B., Banasik, K., Vapnik, Y., and Galuskina, I. (2020) Raman

464   spectroscopy and structural study of baryte-hashemite solid solution from

465   pyrometamorphic rocks of the Hatrurim Complex, Israel. Spectrochimica Acta Part A:

466   Molecular and Biomolecular Spectroscopy.

467 Knops-Gerrits, P.-P., De Vos, D.E., Feijen, E.J.P., and Jacobs, P.A. (1997) Raman

468   spectroscopy on zeolites. Microporous Materials, 8, 3–17.

469 Kolodny, Y., Burg, A., Geller, Y.I., Halicz, L., and Zakon, Y. (2014) Veins in the combusted

470   metamorphic rocks, Israel; Weathering or a retrograde event. Chemical Geology, 385,

471   140–155.

472 Kraus, W., and Nolze, G. (1996) POWDER CELL – a program for the representation and

473   manipulation of crystal structures and calculation of the resulting X-ray powder patterns.

474   Journal of Applied Crystallography, 29, 301–303.

475 Kurszewski, Ł., Palchik, V., Vapnik, Y., Nowak, K., Banasik, K., Galuskina, I. (2021)

476   Mineralogical, geochemical, and Rock Mechanic Characteristics of Zeolite-Bearing

477   Rocks of the Hatrurim Basin, Israel. Minerals, 11, 1062.

478 Kwon, S., Kim, C., Han, E., Lee, H., Cho, H.S., and Choi, M. (2021) Relationship between

479   zeolite structure and capture capability for radioactive cesium and strontium. Journal of

480   Hazardous Materials, 408, 124419.

481 Lengauer, C. C., Kolitsch, U., Tillmanns, E. (2009) Flörkeite, $K_3Ca_2Na[Al_8Si_8O_{32}] \cdot 12H_2O$, a

482   new phillipsite-type zeolite from the Bellerberg, East Eifel volcanic area, Germany.

483   European Journal of Mineralogy, 21, 901-913.

484 Loewenstein, W. (1954) The distribution of aluminum in the tetrahedra of silicates and

485   aluminates. American Mineralogist, 39, 92–69.

486 Mandarino, J.A. (1981) The Gladstone-Dale relationship. IV. The compatibility concept and

487   its application. Canadian Mineralogist, 19, 441–450.

488 Mimura, H., and Akiba, K. (1993) Adsorption Behavior of Cesium and Strontium on

489   Synthetic Zeolite P. Journal of Nuclear Science and Technology, 30, 436–443.

490 Miyawaki, R., Hatert, F., Pasero, M., Mills, S. (2021) Newsletter 63. Mineralogical

491   Magazine, 1-6. doi:10.1180/mgm.2021.74

20

492   Mozgawa, W., Jastrzębski, W., and Handke, M. (2005) Vibrational spectra of D4R and D6R

493   structural units. Journal of Molecular Structure, 744–747, 663–670.

494   Novikov, I., Vapnik, Y., and Safonova, I. (2013) Mud volcano origin of the Mottled Zone,

495   South Levant. Geoscience Frontiers, 4, 597–619.

496   Ori, S., Quartieri, S., Vezzalini, G., and Dmitriev, V. (2008) Pressure-induced over-hydration

497   and water ordering in gismondine: A synchrotron powder diffraction study. American

498   Mineralogist, 93, 1393–1403.

499   Passaglia, E. (1970) The crystal chemistry of chabazites. American Mineralogist, 55, 1278-

500   1301.

501   Passaglia, E., and Sheppard, A. (2001) The Crystal Chemistry of Zeolites. In Natural Zeolites:

502   Occurrence, properties, applications Vol. 45, pp. 69–116. Mineralogical Society of

503   America; Geochemical Society.

504   Sharygin, V.V., Sokol, E.V., and Vapnik, Ye. (2008) Minerals of the pseudobinary

505   perovskite-brownmillerite series from combustion metamorphic larnite rocks of the

506   Hatrurim Formation (Israel). Russian Geology and Geophysics, 49, 709–726.

507   Sharygin, V.V., Lazic, B., Armbruster, T.M., Murashko, M.N., Wirth, R., Galuskina, I.O.,

508   Galuskin, E.V., Vapnik, Y., Britvin, S.N., and Logvinova, A.M. (2013) Shulamitite

509        $Ca_3TiFe^{3+}AlO_8$ - a new perovskite-related mineral from Hatrurim Basin, Israel. European

510   Journal of Mineralogy, 25, 97–111.

511   Sheldrick, G.M. (2008) A short history of *SHELX*. Acta Crystallographica Section A

512   Foundations of Crystallography, 64, 112–122.

513   Sheldrick (2015) Crystal structure refinement with *SHELXL*. Acta Crystallographica Section

514   C Structural Chemistry, 71, 3–8.

515   Smith, J.V. (1988) Topochemistry of zeolites and related materials. 1. Topology and

516   geometry. Chemical Reviews, 88, 149–182.

517   Sokol, E., Novikov, I., Zateeva, S., Vapnik, Ye., Shagam, R., and Kozmenko, O. (2010)

518   Combustion metamorphism in the Nabi Musa dome: new implications for a mud volcanic

519   origin of the Mottled Zone, Dead Sea area: Combustion metamorphism in the Nabi Musa

520   dome. Basin Research, 22, 414–438.

521   Sokol, E., Kokh, S., Sharygin, V., Danilovsky, V., Seryotkin, Y., Liferovich, R.,

522   Deviatiiarova, A., Nigmatulina, E., and Karmanov, N. (2019) Mineralogical Diversity of

523   Ca_2SiO_4-Bearing Combustion Metamorphic Rocks in the Hatrurim Basin: Implications

524   for Storage and Partitioning of Elements in Oil Shale Clinkering. Minerals, 9, 465.

525   Sokol, E.V., Novikov, I.S., Zateeva, S.N., Sharygin, V.V., and Vapnik, Ye. (2008)

526   Pyrometamorphic rocks of the spurrite-merwinite facies as indicators of hydrocarbon

527   discharge zones (the Hatrurim formation, Israel). Doklady Earth Sciences, 420, 608–614.

528   Sokol, E.V., Kokh, S.N., Vapnik, Y., Thiery, V., and Korzhova, S.A. (2014) Natural analogs

529   of belite sulfoaluminate cement clinkers from Negev Desert, Israel. American

530   Mineralogist, 99, 1471–1487.

531   Taylor, A.M. (1964) Zeolite studies IV: Na-P zeolites and the ion exchanged derivatives of

532   tetragonal Na-P. American Mineralogist, 49, 656–682.

533   Tsai, Y.L., Huang, E., Li, Y.-H., Hung, H.-T., Jiang, J.-H., Liu, T.-C., Fang, J.-N., and Chen,

534   H.-F. (2021) Raman Spectroscopic Characteristics of Zeolite Group Minerals. Minerals,

535   11, 167.

536   Vapnik, Y., Sharygin, V.V., Sokol, E.V., and Shagam, R. (2007) Paralavas in a combustion

537   metamorphic complex Hatrurim Basin, Israel. In Geology of Coal Fires: Case Studies

538   from Around the World. Geological Society of America.

539   Vezzalini, G., and Oberti, R. (1984) The crystal chemistry of gismondines : the non-existence

540   of K-rich gismondines. Bulletin de Minéralogie, 107, 805–812.

541   Vezzalini, G., Quartieri, S., and Alberti, A. (1993) Structural modifications induced by

542   dehydration in the zeolite gismondine. Zeolites, 13, 34–42.

543   Wadoski-Romeijn, E., and Armbruster, T. (2013) Topotactic transformation and dehydration

544   of the zeolite gismondine to a novel Ca feldspar structure. American Mineralogist, 98,

545   1988–1997.

546   Yu, Y., Xiong, G., Li, C., and Xiao, F.-S. (2001) Characterization of aluminosilicate zeolites

547   by UV Raman spectroscopy. Microporous and Mesoporous Materials, 46, 23–34.

548

Table 1. Zeolite species with gismondine (**GIS**) framework structure

Name	Gismondine-Ca	Gismondine-Sr	"Gismondine–Ba"	Garronite–Ca	Garronite–Na	Amicite	Gobbinsite
IMA Formula	$Ca_2(Al_4Si_4O_{16})$ $\cdot 8H_2O$	$Sr_4(Al_8Si_8O_{32})$ $\cdot 9H_2O$	$Ba_4(Al_8Si_8O_{32})$ $\cdot 12H_2O$	$Ca_3(Al_6Si_{10}O_{32})$ $\cdot 14H_2O$	$Na_6(Al_6Si_{10}O_{32})$ $\cdot 8.5H_2O$	$K_2Na_2(Al_4Si_4O_{16})$ $\cdot 5H_2O$	$Na_5(Al_5Si_{11}O_{32})$ $\cdot 11H_2O$
Space Group	$P2_1/c$	$B22_12$	*monoclinic*	*I-4m2*	*I2*	*I2*	*Pmn2_1*
a (Å)	10.02	13.794	14.896	9.927	9.990	10.226	10.104
b (Å)	10.62	14.026	9.951	9.927	10.032	10.422	9.782
c (Å)	9.84	10.459	7.613	10.303	10.036	9.884	10.152
α (°)	90	90	90	90	90	90	90
β (°)	92.42	90	103.25	90	90.11	88.32	90
γ (°)	90	90	90	90	90	90	90
V (Å^3)	1046.2	2023.44	1098.42	1015.3	1005.8	1051.7	1003.4
References	(Fischer 1963; Grice et al. 2016)	This work	(Braithwaite et al. 2001; Grice et al. 2016)	(Grice et al. 2016)	(Grice et al. 2016)	(Alberti and Vezzalini 1979; Grice et al. 2016)	(Gatta et al. 2010)

24

550

Table 2. Chemical composition of gismondine-Sr

Constituent	C1			C2		
	mean n=14	s.d	Range	mean n=7	s.d	Range
SiO_2, wt%	34.93	0.56	34.14-36.02	35.37	0.64	34.10-35.89
Al_2O_3	28.99	0.38	28.61-29.96	29.53	0.48	28.59-30.14
CaO	4.38	0.43	3.75 -5.49	4.73	0.23	4.39-5.03
SrO	15.06	0.62	14.10 - 16.57	13.56	0.75	12.14-14.42
BaO	0.26	0.11	0.08 -0.50	0.39	0.08	0.29-0.50
Na_2O	1.38	0.25	0.80 - 1.83	1.13	0.19	0.89-1.39
K_2O	2.45	0.35	1.42 - 2.84	2.77	0.13	2.66-3.03
H_2O	11.66			11.84		
Total	**99.11**			**99.32**		
Si	8.09			8.06		
Al	7.91			7.94		
T	16.00			16.00		
Sr	2.02			1.79		
Ca	1.09			1.15		
Ba	0.02			0.03		
K	0.72			0.81		
Na	0.62			0.50		
Extraframe work cations	4.47			4.28		
H_2O	**9.00**			**9.00**		
R	**0.51**			**0.50**		
E %	**4.08**			**9.66**		

Note: s.d – standard deviation, C1 = Halamish locality; C2 = Zohar locality;
$R = \frac{Si}{Si+Al+Fe}$; E-balance error = $\frac{Al+Fe^{3+}-Al_{theor.}}{Al_{theor.}} \times 100$, $Al_{theor.}$=K+Na+2Ca+2Sr+2Ba
(Passaglia 1970); water content was calculated based on the SC-XRD data.

551

552

553

554

555

556   Table 3. Observed frequencies and their assignments in Raman spectra of gismondine-Sr

Raman bands (in cm^{-1})	Assignments
323, 396, 444, 465, 499, 500	symmetric bending vibrations of T—O—T
677, 702, 721	symmetric stretching modes T—O—T
969,975, 1011, 1012, 1078, 1083	symmetric and antisymmetric stretching vibrations of T—O in tetrahedra
1658, 1661	bending vibrations of water molecules
3131, 3258, 3263, 3396, 3396, 3406, 3466, 3476, 3537, 3572	stretching vibrations of water molecules

557

558   Table 4. Parameters for X-ray data collection and crystal structure refinement.

Crystal data	
Empirical formula	$Sr_{4.99}Ca_{1.52}K_{1.78}Na_{1.46}Si_{16}Al_{16}O_{82.36}$
Crystal system	Orthorhombic
Space group	$B22_12$
Unit cell dimensions [Å]	$a = 14.0256(2)$ $b = 10.45900(10)$ $c = 13.79360(10)$
Volume [Å^3]	2023.44(4)
Z	1
Structure refinement	
Reflections collected	11164
Independent reflections	2171
Observed Data [$I>2\sigma(I)$]	2133
R_1, wR_2 [$I>2\sigma(I)$]	0.0353 (wR = 0.0988)
R_1, wR_2 (for all)	0.0359 (wR = 0.0996)
GooF	1.085
$\Delta\rho_{min}$ [e/Å^{-3}]	-0.34
$\Delta\rho_{max}$ [e/Å^{-3}]	0.72

559

560

561

562
563

564 Table 5. Atom coordinates (x,y,z), equivalent isotropic displacement parameters (U_{iso}, Å^2) and
565 site occupancies.
566

Site	Atom	x	y	z	U_{eq}/U_{iso} [Å^2]	Occupancy
*C*1	Sr	-0.1760(3)	-0.2145(2)	0.09992(19)	0.0305(9)	0.311(8)
*C*1A	Ca	-0.227(3)	-0.179(3)	0.1148(15)	0.049(9)	0.088(13)
*C*1B	Na	-0.203(3)	-0.202(4)	0.063(4)	0.100	0.18(2)
*C*1C	K	-0.148(2)	-0.293(4)	0.105(2)	0.100	0.113(7)
*C*2	Sr	-0.39918(16)	0.0323(2)	0.18035(18)	0.0385(10)	0.312(5)
*C*2A	Ca	-0.3805(8)	0.0744(11)	0.2377(9)	0.025(5)	0.101(9)
*C*2B	K	-0.428(3)	0.043(3)	0.226(3)	0.096(14)	0.107(15)
Si1	Si	0.0000	0.0000	0.43045(11)	0.0132(3)	1
Si2	Si	-0.23632(8)	0.28200(11)	0.16565(8)	0.0129(3)	1
Si3	Si	0.0000	0.0000	0.09934(11)	0.0134(4)	1
Al1	Al	-0.07829(13)	0.2500	0.0000	0.0138(4)	1
Al2	Al	0.10644(13)	0.2500	0.5000	0.0148(4)	1
Al3	Al	-0.15755(9)	0.03249(12)	0.26528(9)	0.0139(3)	1
O1	O	-0.1444(3)	0.3011(4)	0.0980(3)	0.0355(10)	1
O2	O	0.0954(3)	0.0120(4)	0.1624(3)	0.0292(8)	1
O3	O	-0.0876(3)	0.0519(4)	0.3665(3)	0.0316(9)	1
O4	O	-0.3285(3)	0.2375(4)	0.1060(3)	0.0315(9)	1
O5	O	-0.2179(3)	0.1760(4)	0.2489(3)	0.0330(9)	1
O6	O	-0.2443(3)	-0.0838(4)	0.2785(3)	0.0296(8)	1
O7	O	0.0025(3)	-0.1251(4)	0.0313(2)	0.0275(8)	1
O8	O	0.0350(2)	0.1143(4)	0.5004(3)	0.0276(8)	1
*W*1	O	-0.3975(9)	0.0528(12)	0.3721(8)	0.066(4)	0.545(18)
*W*1A	O	-0.5000	0.0000	0.344(3)	0.073(15)	0.23(3)
*W*2	O	-0.2518(13)	-0.0228(18)	0.0161(13)	0.076(8)	0.350(19)
*W*3	O	-0.4874(10)	0.2274(15)	0.2498(10)	0.049(5)	0.359(17)
*W*4	O	-0.3740(16)	-0.1865(19)	0.1058(17)	0.053(7)	0.33(3)
*W*4A	O	-0.345(2)	-0.210(3)	0.068(3)	0.048(11)	0.20(3)
*W*4B	O	-0.351(4)	-0.2500	0.0000	0.08(2)	0.21(4)
*W*4C	O	-0.441(2)	-0.126(3)	0.168(2)	0.083(10)	0.28(2)

567

568

569

570

571

572

27

573   Table 6. Selected interatomic distances (Å).

Site 1	Site 2	Distance (Å)	Site 1	Site 2	Distance (Å)
Si1	O3	1.607(4)×2	Al1	O1	1.724(4)×2
	O8	1.613(4)×2		O7	1.739(4)×2
	mean	1.610		mean	1.732
Si2	O1	1.604(4)	Al2	O8	1.737(4)×2
	O4	1.602(4)		O4	1.729(4)×2
	O6	1.624(4)		mean	1.733
	O5	1.617(4)	Al3	O3	1.719(4)
	mean	1.612		O6	1.730(4)
Si3	O2	1.601(4)×2		O2	1.729(4)
	O7	1.611(4)×2		O5	1.738(4)
	mean	1.606		mean	1.729
*C*1	*W*1	2.670(13)	*C*2	*W*1	2.654(12)
	*W*2	2.548(18)		*W*1A	2.68(4)
	*W*4	2.79(2)		*W*3	2.571(15)
	*W*4A	2.41(3)		*W*4	2.53(2)
	*W*4B	2.84(4)		*W4C*	*1.76(3)*
	O2	2.550(5)		*W*4C	2.45(3)
	O5	2.806		O8	2.783(5)
	O7	2.835		mean	2.490
	mean	2.635	*C*2A	*W1*	*1.883(17)*
*C*1A	*W*2	2.16(3)		*W*3	2.200(19)
	*W*4	2.07(4)		*W*1A	2.36(3)
	W4A	*1.80(4)*		*W*4C	2.45(3)
	*W*4B	2.47(4)		*W*4C	2.74(3)
	O2	2.624(19)		mean	2.327
	mean	2.225	*C*2B	*W*1	2.06(4)
*C*1B	*W4A*	*1.99(5)*		*W1A*	*1.96(6)*
	W2	2.10(5)		*W*3	2.13(4)
	W4B	2.30(7)		*W4C*	*1.94(5)*
	W4	2.47(5)		W4C	2.18(5)
	W4A	2.84(7)		mean	2.054
	mean	2.34	*C*2	*C*2A	*0.942(12)*
*C*1C	*W*1	*1.77(4)*		*C*2B	*0.76(5)*
	*W*2	2.94(4)		*C*2B	2.62(5)
	*W*3	2.77(3)	*C*2B	*C*2	2.62(5)
	*W*4A	2.94(5)		*C*2A	2.95(6)
	O5	2.77(3)		*C*2B	2.20(10)
	mean	2.638	*C*2A	*C*2B	*0.77(4)*
*C*1	*C*1A	*0.83(4)*		*C*2B	2.95(6)
	C1B	*0.65(5)*		*C*1C	2.61(4)
	*C*1B	2.44(5)	*C*1B	*C*1	2.44(5)
	*C*1C	*0.91(4)*		*C*1A	2.77(7)
*C*1A	*C*1B	*0.82(5)*		*C*1B	2.01(10)
	*C*1B	2.77(7)		*C*1C	*1.35(6)*
	*C*1C	*1.63(6)*		*C*1C	2.45(6)
	Si2	3.10(2)			

28

*C*1C	*C*1B	2.45(6)
	*C*2A	2.61(4)
	*C*1	2.86(3)

Note: Non-occurring short distances are reported in italic

574

575 Table 7. Comparison parameters of gismondine-Sr structure

576 with literature data for gismondine-Ca

	Gismondine-Sr This work	Gismondine-Ca (Wadoski-Romeijn and Armbruster 2013)		Gismondine-Ca 75°C (Wadoski-Romeijn and Armbruster 2013)	
Lattice parameteres					
Chemical formula	$Sr_4(Si_8Al_8O_{32})$ $\cdot 9H_2O$	$Ca_4(Si_8Al_8O_{32})$ $\cdot 18H_2O$		$Ca_4(Si_8Al_8O_{32})$ $\cdot 12H_2O$	
Space group	*B22₁2*	*P2₁/c*		*P2₁2₁2₁*	
a	14.0256(2)	10.0214(1)		10.1035(15)	
b	10.45900(10)	10.5997(1)		9.7819(10)	
c	13.79360(10)	9.8327(1)		10.1523(9)	
β		92.363			
V	2023.44(4)	1043.58(2)		1985.6(2)	
Channels size					
[101]		[100]		[101]	
O5-O7	2.90	O8-O8	2.70	O16-O12	2.62
O2-O1	4.57	O3-O3	4.90	O5-O4	4.72
Ellipticity ratio	0.63		0.55		0.55
[10-1]		[001]		[10-1]	
O6-O8	2.91	O7-O6	3.14	O2-O14	2.90
O4-O3	4.58	O2-O4	4.49	O7-O10	4.466
Ellipticity ratio	0.64	Ellipticity ratio	0.70	Ellipticity ratio	0.62
T-O-T angle of the cranckshaft chain					
Si3-O7-Al1	140.21	Si2-O5-Al1	146.54	Si1-O12-Al2	143.68
Si1-O8-Al2	141.19	Si2-O6-Al1	145.75	Si4-O14-Al4	143.52
Si2-O6-Al3	140.84	Si1-O7-Al2	142.43	Si4-O11-Al1	137.14
Si2-O5-Al3	139.67	Si1-O8-Al2	138.55	Si3-O8-Al3	133.32
				Si2-O16-Al1	129.16
				Si2-O2-Al2	130.53
				Si2-O15-Al4	143.30
				Si3-O13-Al3	142.19
mean T-O-T angle	140.47	mean T-O-T angle	143.32	mean T-O-T angle	137.85

Note: Channel sizes were measured according to the free diameter reported in the Atlas of Zeolites Framework Types ellipticity ratio was measured using the free diameter as the ratio of the short diagonal to the long diagonal (Baerlocher et al 2007).

577

29

578   Table S1. Calculated powder diffraction pattern of orthorombic gismondine-Sr (Cu$K\alpha$ =
579   1.540598Å radiation, Debye-Scherrer geometry, $I>2$; Kraus and Nolze 1996)

I	d_{cal}	h	k	l	I	d_{cal}	h	k	l
34	7.1647	1	1	1	8	3.2860	1	3	-1
34	7.1647	1	1	-1	4	3.2860	1	3	1
17	7.1647	1	1	1	4	3.2860	1	3	-1
17	7.1647	1	1	-1	**47**	**3.1281**	**3**	**1**	**3**
2	6.8968	0	0	2	**47**	**3.1281**	**3**	**1**	**-3**
4	5.8247	2	1	0	23	3.1281	3	1	3
3	5.7577	0	1	2	23	3.1281	3	1	-3
100	**4.9173**	**2**	**0**	**2**	4	2.9948	4	1	2
50	**4.9173**	**2**	**0**	**2**	4	2.9948	4	1	-2
6	4.6173	1	2	1	2	2.9948	4	1	2
5	4.6173	1	2	-1	2	2.9948	4	1	-2
3	4.6173	1	2	1	6	2.9674	2	1	-4
3	4.6173	1	2	-1	5	2.9674	2	1	4
7	4.4500	2	1	2	3	2.9674	2	1	-4
7	4.4500	2	1	-2	3	2.9674	2	1	4
3	4.4500	2	1	2	6	2.7776	3	2	-3
3	4.4500	2	1	-2	6	2.7776	3	2	3
88	**4.1922**	**2**	**2**	**0**	3	2.7776	3	2	-3
44	**4.1922**	**2**	**2**	**0**	3	2.7776	3	2	3
46	**4.1670**	**0**	**2**	**2**	4	2.7489	5	0	1
23	4.1670	0	2	2	2	2.7489	5	0	1
5	4.0774	3	1	-1	3	2.7251	1	3	-3
5	4.0774	3	1	1	3	2.7251	1	3	3
3	4.0774	3	1	-1	7	2.7069	1	0	5
2	4.0774	3	1	1	3	2.7069	1	0	5
13	4.0315	1	1	3	34	2.6829	4	2	-2
13	4.0315	1	1	-3	34	2.6829	4	2	2
7	4.0315	1	1	3	17	2.6829	4	2	-2
6	4.0315	1	1	-3	17	2.6829	4	2	2
7	3.5823	2	2	2	25	2.6632	2	2	4
7	3.5823	2	2	-2	25	2.6632	2	2	-4
3	3.5823	2	2	2	12	2.6632	2	2	4
3	3.5823	2	2	-2	12	2.6632	2	2	-4
9	3.3792	3	2	1	8	2.6586	5	1	-1
8	3.3792	3	2	-1	8	2.6586	5	1	1
4	3.3792	3	2	1	4	2.6586	5	1	-1
4	3.3792	3	2	-1	4	2.6586	5	1	1
7	3.3529	1	2	-3	9	2.6205	1	1	5
6	3.3529	1	2	3	9	2.6205	1	1	-5
3	3.3529	1	2	-3	5	2.6205	1	1	5
3	3.3529	1	2	3	4	2.6205	1	1	-5
8	3.2860	1	3	1	29	2.6148	0	4	0
14	2.6148	0	4	0	2	1.9972	2	4	4

30

I	d	h	k	l	I	d	h	k	l
6	2.5270	1	4	-1	2	1.9972	2	4	-4
6	2.5270	1	4	1	4	1.9330	5	1	-5
3	2.5270	1	4	-1	4	1.9330	5	1	5
3	2.5270	1	4	1	4	1.8147	6	2	4
6	2.4723	4	3	0	4	1.8147	6	2	-4
3	2.4723	4	3	0	2	1.8045	4	2	-6
3	2.4586	4	0	4	2	1.8045	4	2	6
7	2.4517	0	3	4	2	1.7912	4	4	4
4	2.4517	0	3	4	2	1.7912	4	4	-4
9	2.3934	4	1	-4	3	1.7634	3	5	-3
9	2.3934	4	1	4	3	1.7634	3	5	3
4	2.3934	4	1	-4	2	1.7330	2	5	4
4	2.3934	4	1	4	2	1.7330	2	5	-4
3	2.3882	3	3	-3	3	1.7236	7	3	-1
3	2.3882	3	3	3	3	1.7236	7	3	1
3	2.3759	3	0	5	3	1.7028	1	3	-7
4	2.2515	3	4	-1	3	1.7028	1	3	7
4	2.2515	3	4	1	3	1.6430	2	6	-2
3	2.2436	1	4	3	3	1.6430	2	6	2
3	2.2436	1	4	-3	14	1.6391	6	0	6
4	2.2139	6	0	2	7	1.6391	6	0	6
2	2.2139	6	0	2	6	1.3888	6	4	-6
3	2.1845	2	0	6	6	1.3888	6	4	6
4	2.0961	4	4	0	3	1.3888	6	4	-6
2	2.0961	4	4	0	3	1.3888	6	4	6
4	2.0835	0	4	4	2	1.2609	10	2	4
4	2.0055	4	4	-2					
3	2.0055	4	4	2					

580

Table S2. Calculated powder diffraction pattern of monoclinic gismondine-Ca (Cu$K\alpha$ = 1.540598Å; Wadoski-Romeijn and Armbruster 2013).

I	d_{cal}	h	k	l	I	d	h	k	l
5	10.0129	1	0	0	3	1.8527	-5	1	2
61	7.2788	1	1	0	5	1.8491	2	3	4
14	7.2054	0	1	1	5	1.8245	-1	2	5
12	5.9342	-1	1	1	14	1.8197	4	4	0
24	5.7664	1	1	1	5	1.8013	0	4	4
2	5.2998	0	2	0	4	1.7996	1	2	5
10	5.0064	2	0	0	3	1.7895	3	5	0
74	4.9122	0	0	2	9	1.7796	0	5	3
19	4.6644	0	2	1	4	1.7784	2	1	5
6	4.4838	-1	0	2	2	1.7666	0	6	0
11	4.4568	0	1	2	3	1.7599	-4	3	3
3	4.3399	1	0	2	3	1.7537	3	5	1
97	4.2602	-1	2	1	17	1.7525	-3	3	4

31

I	d	h	k	l	I	d	h	k	l
37	4.1968	1	2	1	4	1.7233	-4	4	2
30	4.1709	-2	1	1	2	1.7181	4	0	4
4	4.1295	-1	1	2	2	1.711	1	6	1
26	4.0544	2	1	1	3	1.7077	2	2	5
6	4.0163	1	1	2	2	1.7075	4	3	3
3	3.6394	2	2	0	9	1.7008	3	3	4
4	3.6027	0	2	2	2	1.69	4	4	2
4	3.5809	-2	0	2	3	1.6789	2	4	4
4	3.4466	-2	2	1	18	1.6688	6	0	0
13	3.4231	-1	2	2	5	1.6659	2	6	0
6	3.3799	2	2	1	3	1.6624	0	6	2
5	3.3577	1	2	2	2	1.6436	-1	6	2
24	3.3319	1	3	0	5	1.64	-3	2	5
21	3.3248	0	3	1	8	1.6374	0	0	6
100	3.1835	3	1	0	2	1.6362	1	6	2
76	3.1289	0	1	3	2	1.6182	0	1	6
2	3.064	-3	1	1	4	1.6078	-1	1	6
5	3.0205	-1	1	3	3	1.6031	-4	5	1
16	2.9942	3	1	1	3	1.5997	5	2	3
3	2.8683	0	3	2	2	1.5872	3	2	5
2	2.8242	3	2	0	2	1.5783	0	4	5
4	2.8151	-3	0	2	2	1.567	-5	1	4
3	2.7859	0	2	3	6	1.5467	-3	6	1
4	2.7752	-1	3	2	2	1.541	-1	6	3
2	2.752	2	3	1	6	1.5374	3	6	1
8	2.74	1	3	2	2	1.505	3	3	5
65	2.7398	-3	2	1	4	1.4999	-6	3	1
12	2.7208	-3	1	2	5	1.4972	-6	1	3
6	2.7092	3	0	2	2	1.4972	1	7	0
52	2.7086	-1	2	3	3	1.4966	0	7	1
6	2.7016	-2	1	3	3	1.4856	0	3	6
74	2.6895	3	2	1	3	1.4776	-1	3	6
24	2.6599	1	2	3	2	1.466	-4	5	3
43	2.6499	0	4	0	3	1.449	6	1	3
25	2.6248	3	1	2	3	1.4405	-4	3	5
7	2.6075	2	1	3	3	1.4353	4	5	3
4	2.5585	0	4	1	3	1.4333	3	1	6
13	2.515	-2	3	2	2	1.4201	-3	6	3
5	2.5032	4	0	0	2	1.4176	5	4	3
5	2.4853	-1	4	1	17	1.4121	6	4	0
2	2.4725	1	4	1	2	1.41	6	2	3
3	2.4715	-2	2	3	3	1.3989	3	6	3
6	2.4633	2	3	2	2	1.3969	-4	0	6
2	2.4561	0	0	4	14	1.3929	0	4	6
13	2.4018	0	3	3	4	1.3903	-6	3	3
2	2.3927	0	1	4	3	1.3765	-3	3	6
5	2.3871	-4	1	1	3	1.3751	-7	2	1
4	2.3486	-1	1	4	3	1.3744	0	7	3
11	2.3322	0	4	2	3	1.3515	6	3	3
2	2.3289	-3	1	3	2	1.3448	6	4	2

3	2.2882	-2	4	1	4	1.3388	3	3	6
4	2.2684	2	4	1	3	1.3336	-3	7	2
2	2.2634	4	2	0	2	1.3305	5	2	5
8	2.2419	-2	0	4	2	1.33	2	4	6
10	2.194	4	0	2	2	1.3266	2	1	7
2	2.1934	-2	1	4	4	1.3259	7	3	0
4	2.1927	-1	2	4	3	1.325	0	8	0
2	2.1699	2	0	4	3	1.3218	3	7	2
4	2.1499	3	3	2	3	1.3131	0	8	1
5	2.1301	-2	4	2	2	1.3043	0	3	7
5	2.0984	2	4	2	2	1.2926	-7	3	2
5	2.074	1	5	0	4	1.291	-7	2	3
2	2.0425	4	3	0	2	1.2905	-1	5	6
8	2.0411	-3	4	1	4	1.2809	2	8	0
11	2.0281	-1	4	3	3	1.2747	-3	2	7
11	2.0075	1	4	3	2	1.2547	7	2	3
4	1.9827	-3	1	4	2	1.2506	2	3	7
5	1.9678	5	1	0	2	1.2397	3	2	7
2	1.9642	1	3	4	4	1.2378	-4	1	7
8	1.932	0	1	5	2	1.2357	-4	4	6
2	1.9206	-2	5	1	5	1.2312	-6	5	3
4	1.9181	4	1	3	2	1.2215	-3	5	6
4	1.9114	-1	1	5	2	1.2111	3	6	5
3	1.9089	-4	3	2	3	1.2039	6	5	3
2	1.9088	2	5	1	2	1.1936	-6	0	6
3	1.9087	3	1	4	2	1.1696	6	6	2
2	1.8953	-4	2	3	3	1.1454	6	0	6
4	1.8828	1	1	5	3	1.1083	0	9	3

583

584

585

586

587

588

589

590

591
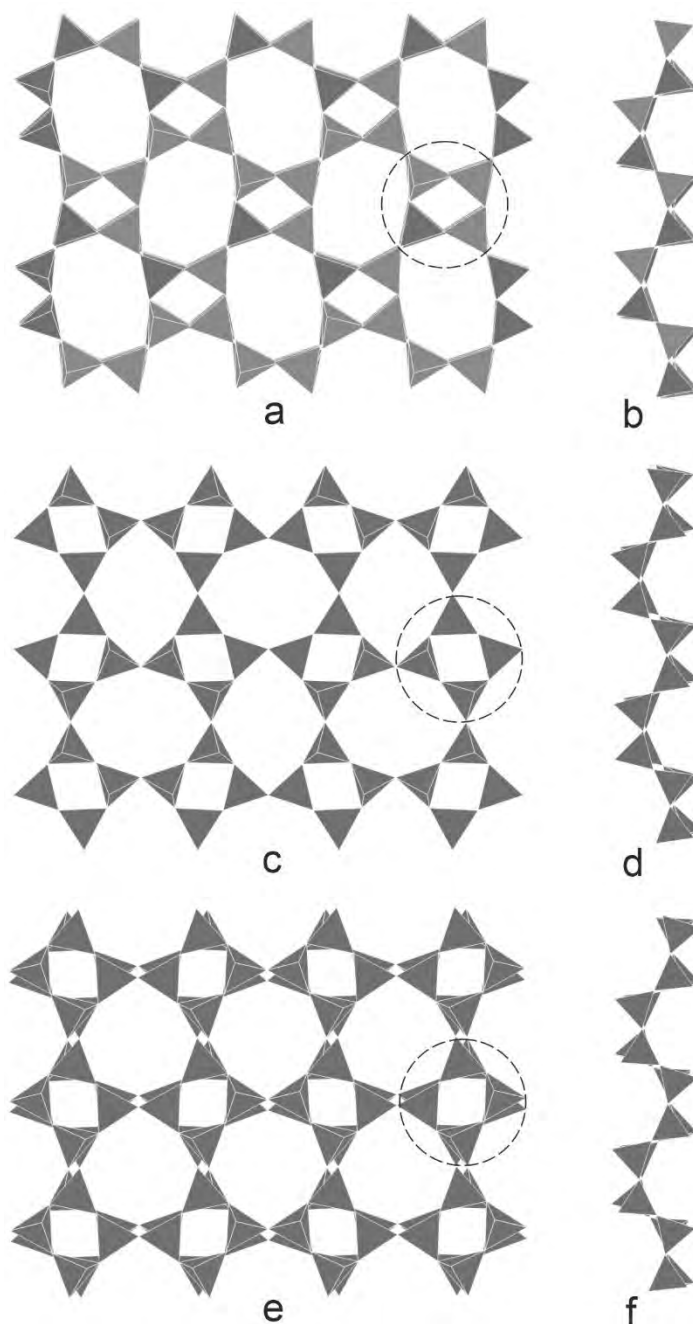
Fig. 1 Zeolites with framework built by double connected 4-member rings: (**a**) **GIS** framework type projected on (100), the dashed circle line point out a double crankshaft chain parallel to [100]; (**b**) double crankshaft chain of **GIS** framework type (gismondine-Ca; Wadoski-Romeijn and Armbruster 2013); (**c**) **MER** framework type projected on (001), the dashed circle line point out a double crankshaft chain parallel to [001]; (**d**) double crankshaft chain of **MER** framework type (merlionite; Galli et al 1979); (**e**) **PHI** framework type projected on (100), the

34

598   dashed circle line point out a double crankshaft chain parallel to [100]; (**f**) double crankshaft

599   chain of **PHI** framework type (phillipsite; Gatta et al 2009).

Figure 2
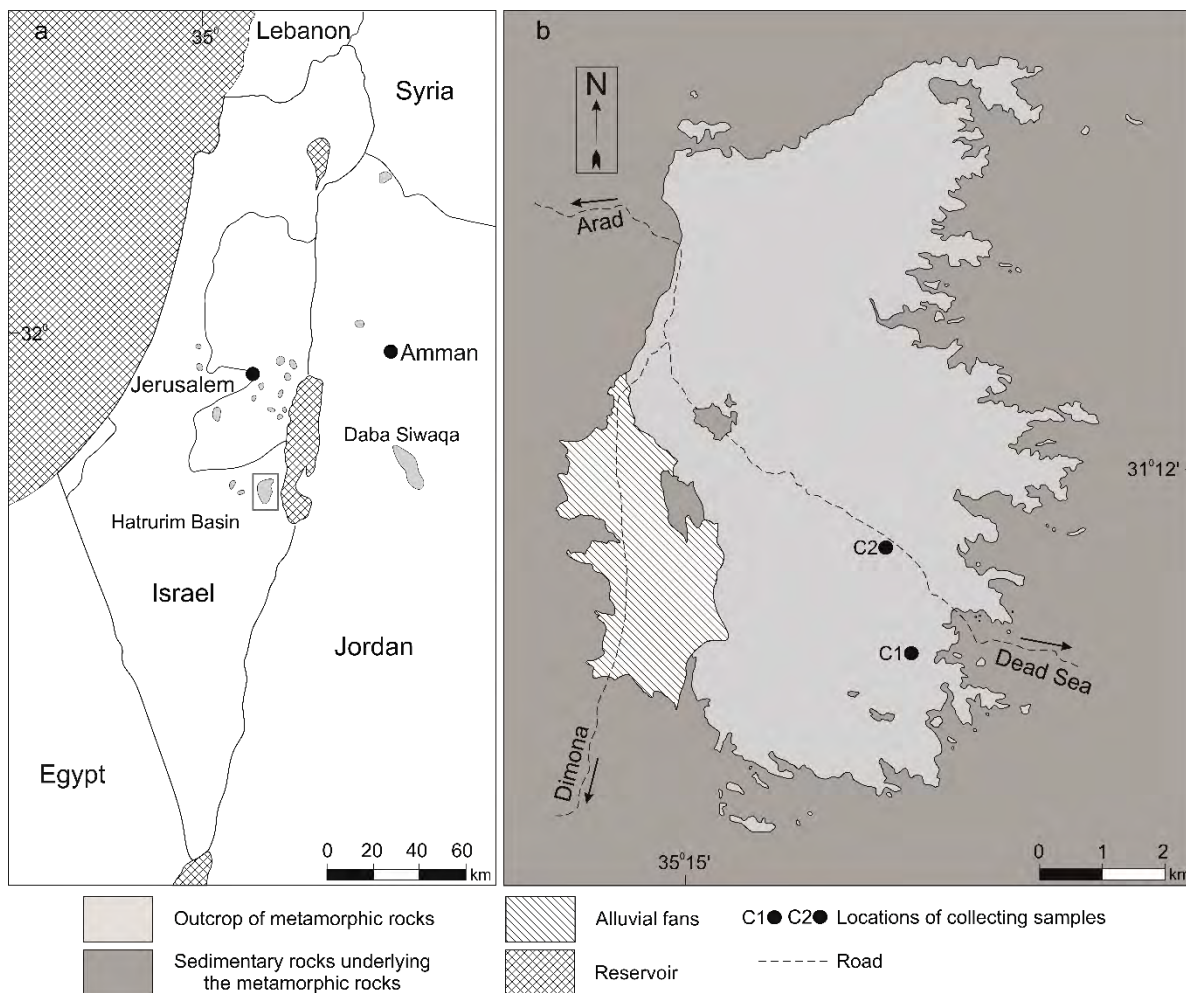
600

601   Fig. 2 (**a**) Schematic map of the pyrometamorphic rocks outcrops in Israel, Palestinian

602   Autonomy and Jordan; Fragment outlined by frame is magnified in Fig. 2b, (**b**) Map of the

603   Hatrurim Basin with marked locations of sampling: wadi Halamish outcrops (C1), wadi Zohar

604   (C2) (Created on the basis of Geological Map of Israel 1:50 000, Arad sheet, Hirsch et al. 2008).

35

Figure 3
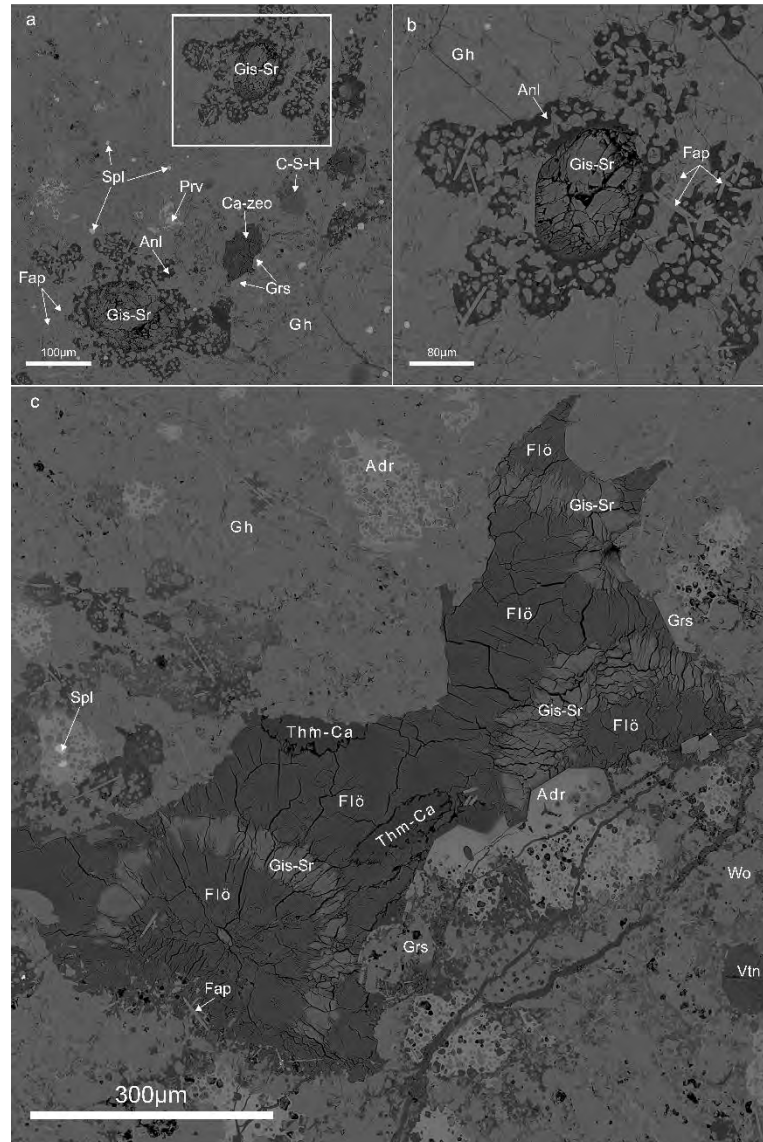
Fig. 3. (**a**) Gehlenite-wollastonite-garnet hornfels with small voids filled by zeolite including

gismondine-Sr. Fragment outlined by frame is magnified in Fig. 3b. (**b**) Gismondine-Sr with

gismondine-Ca (most probably) rim in amygdule, around which analcime occurs with an

irregular distribution. (**c**) Zone of gismondine-Sr in spherulite aggregates between two flörkeite

generations. BSE images.

Anl - analcime, Adr - andradite, Ca-zeo - calcium zeolite, C-S-H - hydrated calcium silicates,

Fap - fluorapatite, Flö - flörkeite, Gh - gehlenite, Grs – grossular, Prv - perovskite, Spl - spinel,

Vtn - vertumnite, Wo - wollastonite, Gis-Sr- gismondine-Sr. Thm-Ca - thomsonite-Ca.

Figure 4
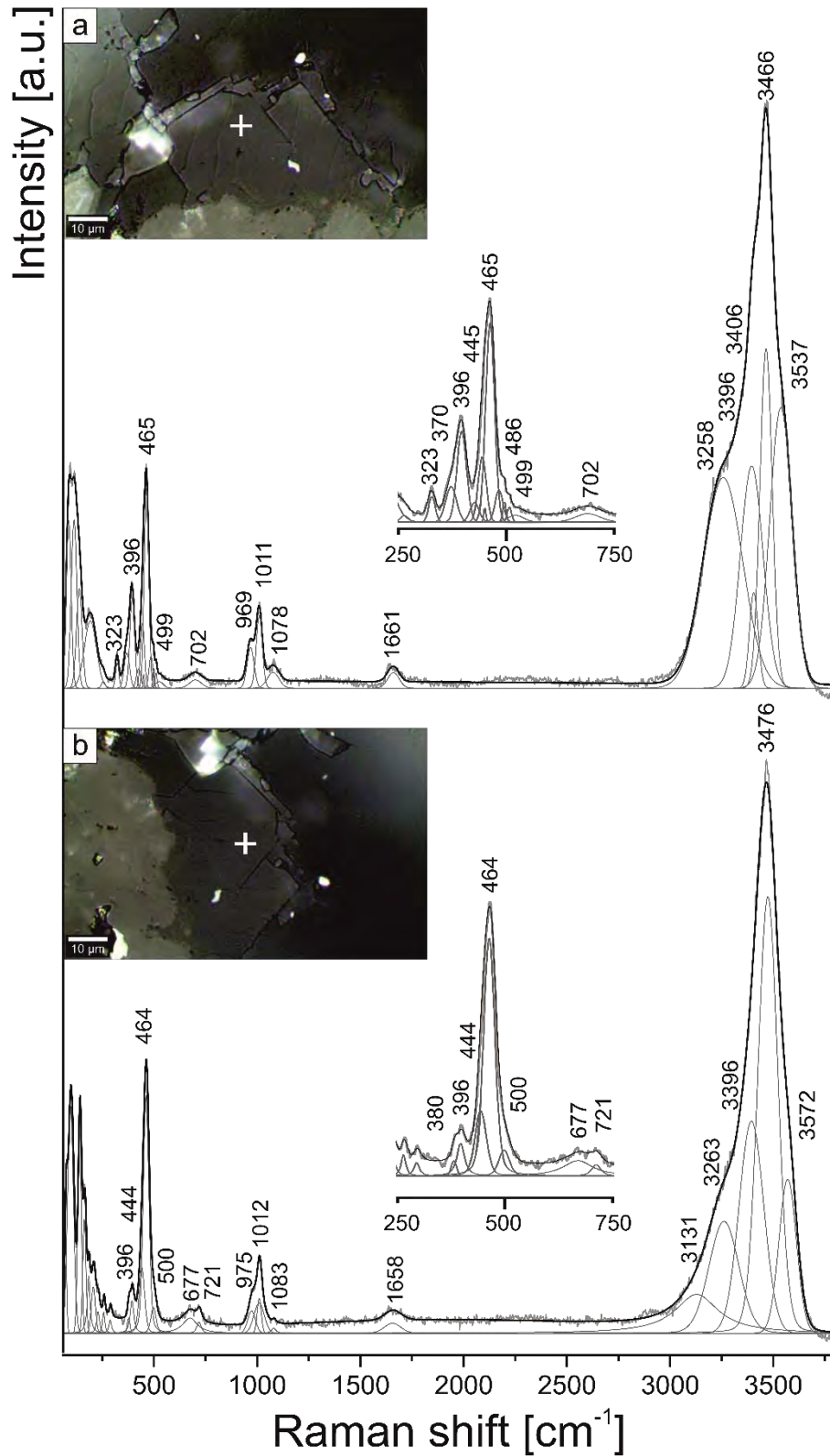
614   Fig. 4 (**a,b**) Raman spectra of gismondine-Sr in two orientations.
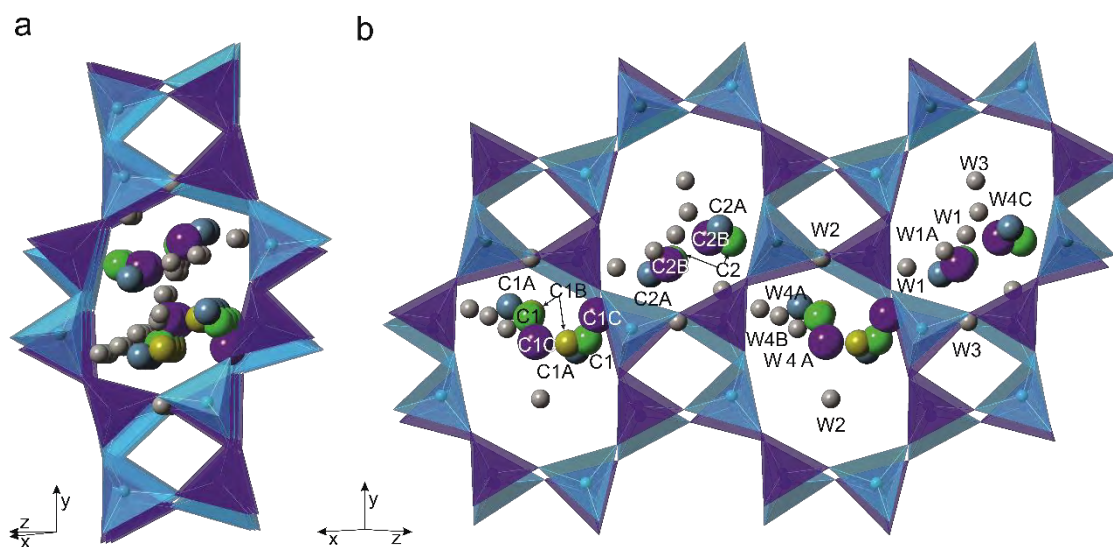
37

Figure 5
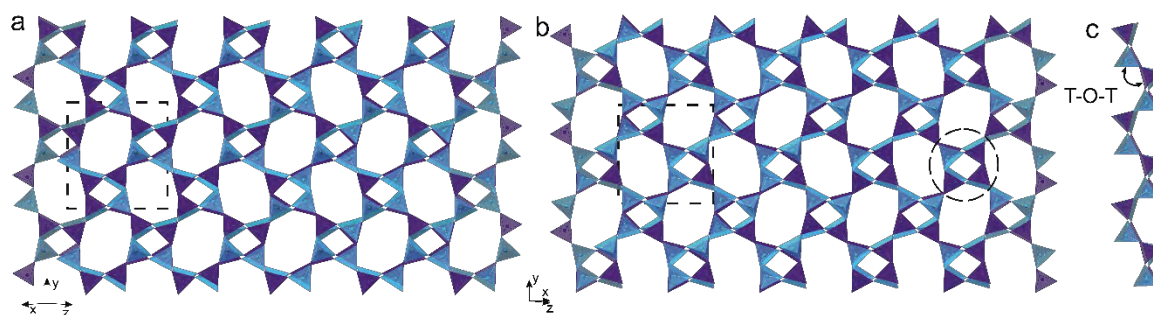
Fig. 5. The framework of gismondine-Sr structure: (**a**) projection on (101); (**b**) projection on (10-1), dashed circle indicates double crankshaft chain (*dcc*); (**c**) *dcc* running parallel to [10-1] with the marked T-O-T angle between the tetrahedra up and down. Silica tetrahedra are dark blue and alumina tetrahedra are light blue, dashed line shows the unit cell.

Figure 6

Fig. 6. (**a**) General view of the 8-membered rings channel, projection along [10-1]. (**b**) Cations and H_2O distributed into 4 adjacent *t-gsm* cavities, projection along [101]. All extraframework sites are partially occupied. Strontium, calcium, potassium, and sodium are represented as green, blue, purple, and yellow spheres, respectively. Grey spheres represent H_2O sites.
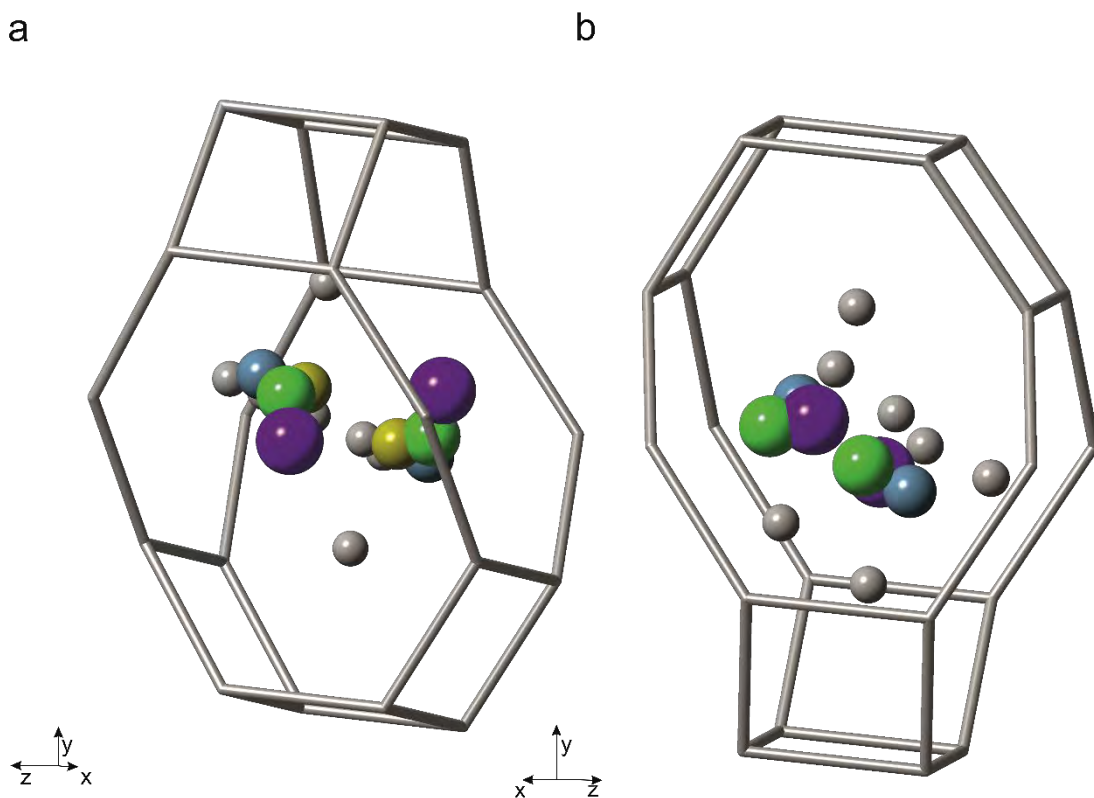
Figure 7

a

b

626

Fig. 7. Exraframework cations population in the two non-equivalent symmetry cages: (**a**) cage containing Ca, K, and Na; (**b**) cage containing Ca and K at $C2A$ and $C2B$ sites. All extraframework sites are partially occupied. Strontium, calcium, potassium, and sodium are represented as green, blue, purple, and yellow spheres, respectively. Grey spheres represent H_2O sites.

Figure 8

632
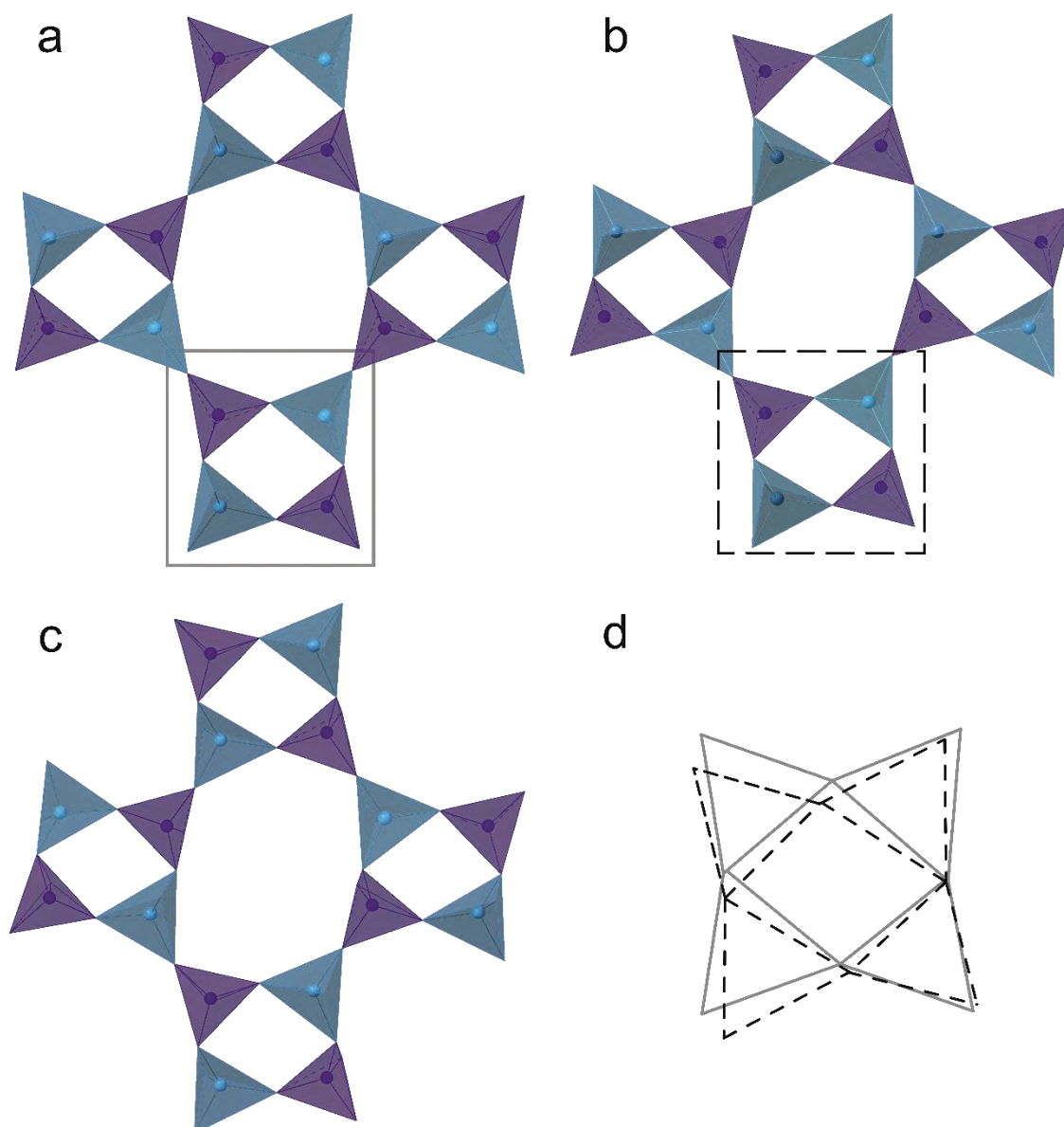
Fig. 8. Part of the framework containing 8- and 4-membered rings : (a) gismondine- Ca projection along [00-1] (Wadoski-Romeijn and Armbruster 2013); (b) Gismondine-Sr projection along [101], (c) Partially dehydrated gismondine-Ca at 75 °C along [101] (Wadoski-Romeijn and Armbruster 2013), (d) scheme of overlapping double 4-memebr ring of gismondine-Ca (gray line) and gismondine-Sr (dashed line).

638